Journal of Physics: Conference Series **2792** (2024) 012006 doi:10.1088/1742-6596/2792/1/012006

Sol gel synthesis of TiO_2@ZnO composites for self-cleaning and antimicrobial coating

D. Bruzl[1], L. Bocian[1], P. Sokola[1], J. Másilko[1], M. Sedlačík[1], J. Švec[1], E. Bartoníčková[1,2] and F. Šoukal[1]

[1] Institute of Materials Science, Faculty of Chemistry, Brno University of Technology, Purkynova 118, Brno, 635 00, Czech Republic
[2] Department of Thermal Engineering, Faculty of Material Science and Technology, VSB-Technical University of Ostrava, 17. Listopadu 2172/15, Ostrava 738 01, Czech Republic

E-mail: bruzl.dominik@gmail.com

Abstract. In recent years, the development of advanced materials for applications in self-cleaning surfaces and antimicrobial coatings has received considerable attention due to its potential impact on environmental sustainability and public health. Among the emerging materials, metal oxide-based photocatalysts have shown promise in addressing these challenges. In this context, the present study focuses on the promise sol-gel synthesis and potential photocatalytic properties of TiO_2@ZnO (x = 0.6 - 0.9) nano-scaled particles, with particular emphasis on their applications in self-cleaning and microbial coatings. The choice of TiO_2@ZnO (x = 0.6 - 0.9) as the subject of investigation is driven by the advantageous properties of both titanium dioxide (TiO_2) and zinc oxide (ZnO). TiO_2 is known for its exceptional photocatalytic activity, while ZnO is known for its antimicrobial properties. By combining these two metal oxides in a controlled manner, we aim to harness their synergistic effects to create a multifunctional material with enhanced performance. A titanium (IV) isopropoxide and zinc acetate dihydrate have been used as precursors for the so-gel process. The synthesised powders were evaluated by X-ray diffraction analysis and Raman spectroscopy to determine the allotropy of TiO_2 and possible lattice distortions. The optical band gap (E_{gap}) was evaluated by molecular reflection UV-VIS spectroscopy. In addition, size and morphology were determined by scanning electron microscopy (SEM).

Introduction

Titanium dioxide (TiO_2) is commonly found in nature as the minerals rutile and anatase (both tetragonal), or ilmenite ($FeTiO_3$), from which it is also industrially produced. Another modification is orthorhombic brookite. Significant reserves of these minerals are found virtually worldwide, particularly in China, furthermore in Australia, North America, Nigeria, Malaysia, Brazil, India and South Africa, and off Earth on the surface of the Moon, where its content is estimated to be up to 12 % [1,2]. An important property of titanium dioxide is the width of the forbidden band (E_g) determining the applicability of TiO_2 in semiconducting components varies based on its crystalline modification, with E_g being 3 eV for rutile and 3.2 eV for anatase, limiting pure titanium dioxide to applications only in the UV region [3]. In order to decrease the band gap value for usage as a photocatalyst in visible light region can be TiO_2 (beside other properties improvements) modified with dopants - WO_3 [4], C_3N_4 [5] or ZnO [6] belongs to the common examples. Doping with precious metals, such as Pt [7], Ag and Au [8] the nanoparticle - sized anatase structures are also interesting options for shift to absorption to VIS region of TiO_2.

Self-cleaning ability of doped TiO_2 nano-scaled particles has been characterized by their capacity to degrade organic matter and also to eliminate microorganisms when exposed to UV/VIS light due to their photocatalytic properties. Doping, such as Zn, can improve light absorption in the visible spectrum and enhance photocatalytic efficiency. These properties make doped TiO_2 nano-scaled particles suitable candidates for applications in self-cleaning surfaces and antimicrobial protective coatings [9,10].

Research on synthesis of anatase nano-scaled particles has been a constant topic of interest for decades. For example, Mustapha et al. [11] synthesized TiO_2 nano-scaled particles by the sol-gel technique from titanium isoproxide and sodium hydroxide precursors and calcined at 450 °C. The effect of solution pH and stirring time on the crystallite size and particle distribution was studied. They found pH 8 and stirring time of 80 min as the optimum conditions. A study by Younis [12] in 2023 investigated the antibacterial properties of TiO_2 nano-scaled particles prepared by sol-gel technique also from Ti-isoproxide, under the choice of two calcination temperatures (500 °C for anatase particles and 900 °C for rutile particles). The synthesized particles reached particle sizes of 300 ± 100 nm and tended to aggregate. In his study, Javed [13] doped (among Mg) TiO_2 with zinc (using Ti-isopropoxide and zinc nitrate, the gel was allowed to dry for 24 h at room temperature, and then calcined at 400 °C). The XRD results showed the presence of anatase phase in both pure TiO_2 and doped samples, Raman spectroscopy demonstrated the incorporation of Zn into the TiO_2 structure and the calculated average particle size from SEM images was around 5 nm for pure TiO_2 and below 100 nm for Zn doped TiO_2. The decrease in intensity and FHWM (full width at half maximum) of E_g band width of Zn-doped TiO_2 compared to pure TiO_2 one and its subsequent improvement in photocatalytic properties is reported in other studies [14,15,16].

The aim of this study is to prepare TiO_2 nano-scaled particles doped with zinc ions in the stoichiometric ratio of 0.6 - 0.9 in favor of Ti and their characterization. The particles were synthesized by sol-gel process to achieve nanosized powders with targeted properties.

Experimental

Synthesis of TiO_2 nano-scaled particles

TiO_2 and Zn-doped TiO_2 nano-scaled particles were produced using the sol-gel technique. Initially, 125 ml of isopropanol (Lachner, p.a.) was gradually stirred with 93 ml of titanium (IV) isopropoxide (Sigma Aldrich, < 97 %) and acidified using 1 ml of nitric acid (solution 1). Solution 2 comprised of zinc acetate (Lachema, p.a.) dissolved in 200 ml of deionized water. The concentration of zinc ions was adjusted to achieve stoichiometric ratios of 0.1, 0.2, 0.3, and 0.4 relative to titanium.

Solution 1 and 2 was then dropwise introduced to ammonia solution (Penta, p.a., 125 ml in 375 ml deionized water) leading to the formation of a white precipitate. The mixture was subjected to continuous stirring (at 500 rpm) for a duration of 4 hours and aged for 24 hours. Subsequently formed precipitate was washed to the neutral pH and separated using the centrifugation. The obtained precursor was subsequently dried at temperature 105 °C and calcinated at 550 °C for 2 h within a high-temperature muffle furnace. Obtained products were crushed and milled in mortar for 2 min for further characterization.

Characterization

Morphology of synthetized TiO_2 samples were observed on a scanning electron microscope (EVO LS10 ZEISS). For the analysis the samples were gold-sputtered for one minute on the Au sputter coater instrument (SC7640 Polaron). For taking the images, a voltage of 10 kV, and a current of 100 pA was used. Phase compositions were assessed by XRD measurements (Empyrean diffractometer, Malvern PANalytical). The experimental conditions included a tube current of 30 mA and a voltage of 40 kV, with a copper anode source (Cu Kα1 = 1.540598 Å). The diffractometer was set to a gonio scan axis, covering a 2θ range from 5 to 90 degrees with a step size of 0.01313 Å and a dwell time of 96 seconds per step. Data analysis was performed with HighScore Plus software. The exact content of all phases was calculated for ZnO-doped TiO_2 nano-scaled particles by Rietveld quantitative phase analysis. UV- visible diffusion reflectance spectroscopy (DRS) has been used to determine the band gap energies (E_g) of synthesized pure TiO_2 and ZnO-doped TiO_2 nano-scaled particles. For band gap calculations was used Kubelka - Munk approach. Particles in the form of pressed pellets were measured on a spectrometer (SF 600 PLUS-CT Datacolor) with wavelength range λ = 360-700 nm and resolution of 10 nm. Raman

scattering experiments were conducted using a confocal micro-Raman microscope (NanoFinder S SOL instruments), utilizing a 633 nm excitation wavelength at 10 mW. Calibration was done using silicon at 520.6 cm^{-1}. A 50× objective lens with a 0.8 numerical aperture focused the beam, with each measurement taken over 2 seconds of exposure and a resolution of 0.9 cm^{-1}. These measurements were all carried out at ambient conditions and room temperature.

Results and discussion

Phase composition and crystal structure

Figure 1 shows the XRD pattern of synthesized TiO_2 and TiO_2@ZnO nano-scaled particles in different stoichiometric ratios. The presence of anatase was confirmed in all samples (peak corresponding to $2\theta = 25.3°$). Pure TiO_2 consisted of anatase only. Formation of predominantly anatase phase in non-doped TiO_2 nano-scaled particles was also observed in previous studies [17,18], however if higher temperatures of calcination (above 600 °C) are selected, a rutile phase starts to prevail [19, 20, 21]. The sharpness of the peak is indicative of well-crystallized nano-scaled particles [15]. After doping with zinc, rutile ($2\theta = 27.5°$) and $TiZnO_3$ ($2\theta = 32.8°$ and $35.6°$) phases started to appear in the system, according the TiO_2 – ZnO phase diagram [22]. Corresponding to our founding, in study from Song [23] is stated, that Zn^{2+} ions beside others promote the anatase-rutile (A - R) transformation. By the study also presents, that A-R transformation can be inhibited with addition of Al^{3+}, Cu^{2+} and Co^{2+} ions into the system. The formation of lesser amounts of $Ti_3Zn_2O_8$ ($2\theta = 30.4°$) was also observed in all samples except $Ti_{0.6}Zn_{0.4}O_2$. Formation of this compound in TiO_2 – ZnO system has been already described in this study [24]. A summary of these is given in Table 1.

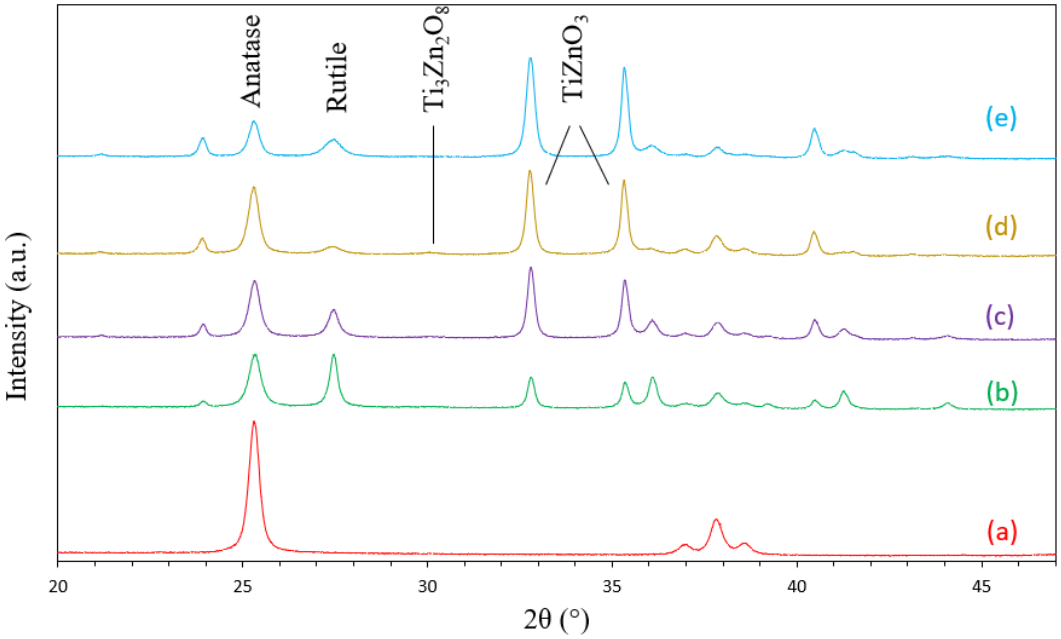

Figure 1. XRD pattern of synthesized pure TiO_2 and TiO_2@ZnO nano-scaled particles: **a** TiO_2 **b** $Ti_{0.9}Zn_{0.1}O_2$, **c** $Ti_{0.8}Zn_{0.2}O_2$ **d** $Ti_{0.7}Zn_{0.3}O_2$ and **e** $Ti_{0.6}Zn_{0.4}O_2$.

Table 1. List of phases and their content presented in synthesized pure TiO_2 and in Zn-TiO_2 systems

Sample	Phase	Content (%)	Crystallite size (nm)
TiO_2	Anatase	100.0	25.0
$Ti_{0.9}Zn_{0.1}O_2$	Anatase	41.0	22.7
	Rutile	40.3	37.4
	$TiZnO_3$	18.3	48.6
	$Ti_3Zn_2O_8$	0.4	-
$Ti_{0.8}Zn_{0.2}O_2$	Anatase	36.8	25.8
	Rutile	23.9	27.9
	$TiZnO_3$	38.5	48.1
	$Ti_3Zn_2O_8$	0.8	-
$Ti_{0.7}Zn_{0.3}O_2$	Anatase	41.7	27.2
	Rutile	9.1	18.3
	$TiZnO_3$	48.0	46.4
	$Ti_3Zn_2O_8$	1.2	-
$Ti_{0.6}Zn_{0.4}O_2$	Anatase	20.0	28.6
	Rutile	20.2	19.0
	$TiZnO_3$	59.8	42.4

The Scherrer equation was used to estimate the crystallite sizes using the most intense reflections for a given phase. The form of the equation is following:

$$L = \frac{K \cdot \lambda}{\beta \cdot cos\,\theta} \quad (1)$$

where L is the average crystallite size, K is Scherrer constant, λ is the X-ray wavelength, β is the linear broadening at FWHM in radians and θ is the Bragg´s angle [25,26].

With the increase of Zn doping, the size of anatase crystallites slightly increased compared to the reference (pure TiO_2, crystallite size 25.0 nm), namely 25.8 nm – 28.6 nm, showing some degree of Zn integration into the TiO_2. The exception was $Ti_{0.9}Zn_{0.1}O_2$ (crystallite size 22.7 nm). The crystallite size of rutile decreased with doping (37.4 nm to 18.3 nm), as was the case for the $TiZnO_3$ phase (48.6 – 42.4 nm respectively). All lattice parameters of synthesized TiO_2 and TiO_2@ZnO nano-scaled particles are given in Table 2. Slight increase in lattice parameter *a* and *b* and decrease in *c* parameter in anatase phase (0.001 Å for *a* and *b* parameters and 0.005-0.007 Å for *c* parameter) in Zn-doped nano-scaled particles compared to pure TiO_2 reference was observed [27,28]. Such lattice parameters confirm the partial integration of Zn^{2+} ions into the TiO_2 structure without significant lattice distortions, which can be attributed to the very similar atomic radii of Zn^{2+} and Ti^{4+} ions (0.74 Å and 0.75 Å as stated Aware [15]).

Table 2. A summary of lattice parameters of pure TiO_2 and ZnO-doped TiO_2 nano-scaled particles.

Sample	Phase	Crystallographic structure	Lattice parameter					
			a (Å)	b (Å)	c (Å)	A (°)	B (°)	γ (°)
TiO_2	Anatase	Tetragonal	3.785	3.785	9.509	90	90	90
$Ti_{0.9}Zn_{0.1}O_2$	Anatase	Tetragonal	3.786	3.786	9.503	90	90	90
	Rutile	Tetragonal	4.593	4.593	2.959	90	90	90
	$TiZnO_3$	Rhombohedral	5.077	5.077	13.929	90	90	120
$Ti_{0.8}Zn_{0.2}O_2$	Anatase	Tetragonal	3.786	3.786	9.503	90	90	90
	Rutile	Tetragonal	4.593	4.593	2.959	90	90	90
	$TiZnO_3$	Rhombohedral	5.077	5.077	13.926	90	90	120
$Ti_{0.7}Zn_{0.3}O_2$	Anatase	Tetragonal	3.786	3.786	9.503	90	90	90
	Rutile	Tetragonal	4.593	4.593	2.959	90	90	90
	$TiZnO_3$	Rhombohedral	5.077	5.077	13.925	90	90	120
$Ti_{0.6}Zn_{0.4}O_2$	Anatase	Tetragonal	3.786	3.786	9.503	90	90	90
	Rutile	Tetragonal	4.593	4.593	2.959	90	90	90
	$TiZnO_3$	Rhombohedral	5.077	5.077	13.927	90	90	120

Raman spectroscopy was used to confirm the targeted incorporation of Zn^{2+} ions into the anatase structure and change band gap to VIS region (See Figure 7 and 8). Collected Raman spectra of samples are given in Figure 2. From XRD analyses was determined presence of anatase, "undesirable" rutile, zinc titanate phases and also is visible presence of rutile in form of multiple E_g peak (Figure 3). There are visible 4 active phonon modes at about 140 cm^{-1} (E_g), 393 cm^{-1} (B_{1g}), 514 cm^{-1} (A_{1g} + B_{1g}) and 636 cm^{-1} (E_{1g}) belong to anatase tetragonal structure *I41/amd* [29,30]. From the Raman spectra can be distinguished peaks belonged to anatase and zinc titanate structure. Figure 3 shows the detail in *Eg* band of anatase prevented in all samples. The shift to the higher values is clearly visible and confirm the suggested of Zn^{2+} ions incorporation to the anatase structure. Peaks 350 cm^{-1} (A_g) and 718 cm^{-1} (A_g) are connected to symmetrical phonon modes of secondary phase rhombohedral $ZnTiO_3$ with space group $R\bar{3}$ *(148)* [29]. Figure 3 shows in detail the symmetrical E_g band of anatase presented in all samples. The shift to the higher values is clearly visible and confirms the suggested of Zn^{2+} ions incorporation to the anatase structure from XRD analysis. With the increasing of Zn^{2+} ions concentrations the undesirable anatase to rutile transformation occurred, which was observed by XRD analysis and confirmed by Raman spectroscopy. Intensity of E_g peak is decreased with increasing Zn doping, which is connected with the change of crystallite size and also with the gradually increasing rutile formation. Even at the low Zn^{2+} concentration (sample $Ti_{0.8}Zn_{0.2}O_2$) the ATR transformation is visible (shoulder around peak 156 cm^{-1}).

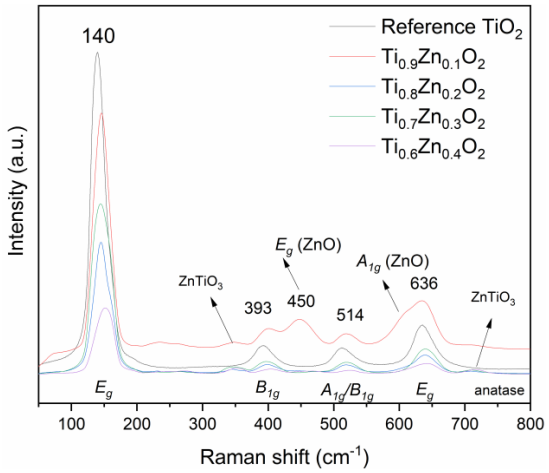

Figure 2. Overall Raman spectra for TiO_2@ZnO composites.

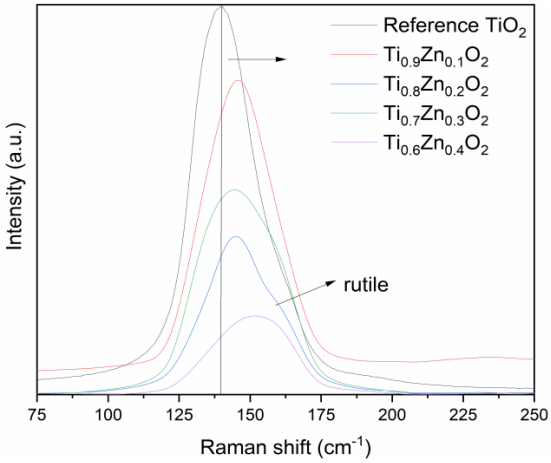

Figure 3. Raman spectra of TiO_2@ZnO composites (in detail E_g band of anatase).

Morphology

The microstructure of TiO_2 (reference) and TiO_2@ZnO composites is given in Figures 4 and 5. It was found that the nanoscale particles were successfully synthesized. As can be seen in Figures 4 and 5, the nano-scaled particles for all samples without additive treatment tend to agglomerate. However, other factors, such as temperature or solvent type, may also influence the degree of agglomeration of the prepared nano-scaled particles [31]. In both cases, the reference, and TiO_2@ZnO samples, it could be observed that the nano-scaled particles merged to the larger (micro-sized) units.

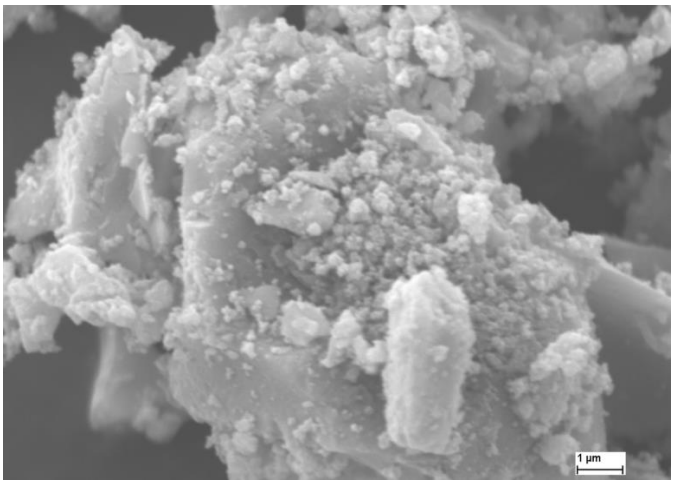

Figure 4. SEM micrographs of the synthesized nano-scaled particles TiO_2 at magnification 25 000×.

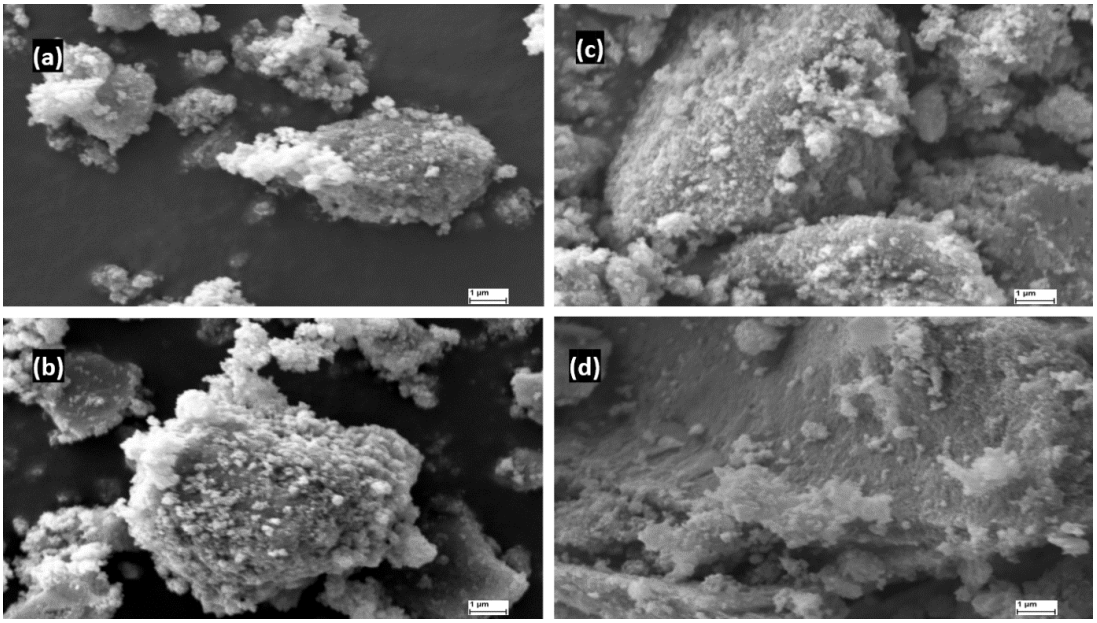

Figure 5. SEM micrographs of the synthesized nano-scaled particles: **a** $Ti_{0.9}Zn_{0.1}O_2$, **b** $Ti_{0.8}Zn_{0.2}O_2$ **c** $Ti_{0.7}Zn_{0.3}O_2$ and **d** $Ti_{0.6}Zn_{0.4}O_2$ at magnification 25 000×.

The observed agglomeration of TiO_2@ZnO nano-scaled particles synthesized by the sol-gel technique is consistent with the findings of previous studies and suggests a reoccurring phenomenon during the formation of nano-scaled particles [15,19]. Electron microscopy with enhanced resolution in these previous studies not only confirmed the agglomeration but also detailed the spherical morphology of the particles, a feature also observed by Kumar [16] and Tamgadge [32]. This spherical shape, consistently observed in

various studies, highlights the natural tendencies in the sol-gel process and contributes to our understanding of nanoparticle aggregation and morphology. The consistency of these observations highlights the importance of microscopic analysis in the characterization of nano-scaled particles and offers insight into structural nuances that significantly affect material properties and potential applications.

Optical properties

Figure 6 shows collected diffusion reflectance spectra of synthesized TiO_2 nano-scaled particles and TiO_2@ZnO particles in different stoichiometric ratios.

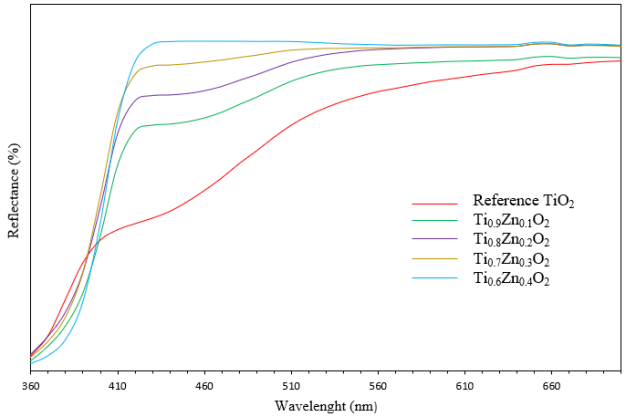

Figure 6. Reflectance spectra for TiO_2@ZnO composites.

The band gap energy (E_g) is calculated using the Kubelka-Munk function and Tauc plot according to the following equations:

$$(F(R_\infty) = \frac{K}{S} = \frac{(1-R_\infty)^2}{2R_\infty} \quad (2)$$

where $R_\infty = \frac{R_{sample}}{R_{standard}}$ is the reflectance of an infinitely thick specimen, while K and S are the absorption and scattering coefficients.

$$(F(R_\infty) \cdot h\nu^{\frac{1}{2}} = B(h\nu - E_g) \quad (3)$$

where h is the Planck constant, ν is the photon´s frequency and B is a constant [15].

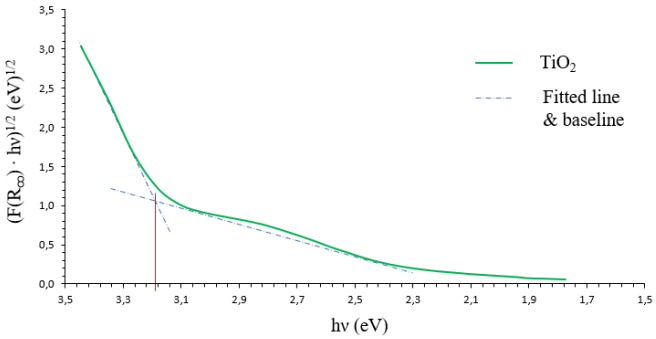

Figure 7. Evaluation of band gap energy (E_g) determination of the synthesized nano-scaled particles TiO_2 from the Tauc plot (the linear part of the plot was extrapolated to the *x*-axis).

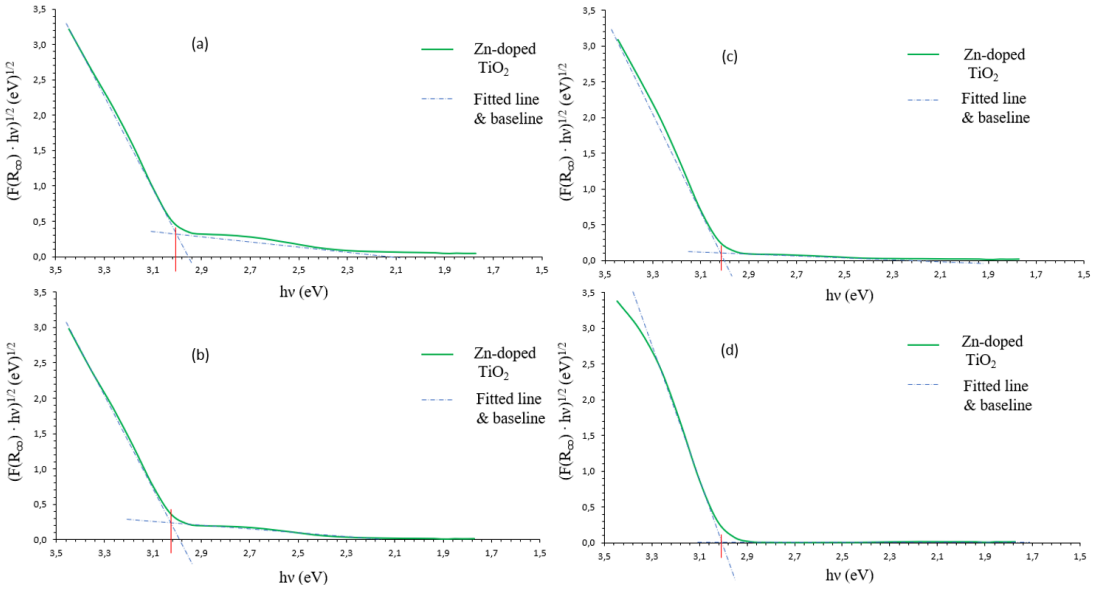

Figure 8. Evaluation of band gap energy (E_g) determination of the synthesized nano-scaled particles: **a** $Ti_{0.9}Zn_{0.1}O_2$, **b** $Ti_{0.8}Zn_{0.2}O_2$ **c** $Ti_{0.7}Zn_{0.3}O_2$ and **d** $Ti_{0.6}Zn_{0.4}O_2$ from the Tauc plot (the linear part of the plot was extrapolated to the *x*-axis).

By extrapolating the linear part of the plot to the *x*-axis, band gap energies have been determined for (see Figures 7 and 8). All ZnO-doped composites had lower band gap energies, than reference sample TiO_2 anatase with E_g = 3.17 eV. A decrease in band-gap energy, up to 3.01 eV, can be attributed to the combined effect of Zn doping and also anatase to rutile A - R transformation. A decrease of TiO_2 band gap energy when Zn doped was also observed in numerous studies [15,33,34]. A summary of all band gap energies is given in Table 3.

Table 3. Determined band gap energies corresponding to synthesized ZnO@TiO_2 composites.

Sample	E_g (eV)
TiO_2	3.18
$Ti_{09}Zn_{01}O_2$	3.01
$Ti_{08}Zn_{02}O_2$	3.02
$Ti_{07}Zn_{03}O_2$	3.02
$Ti_{06}Zn_{04}O_2$	3.01

Conclusion

In the presented work, the sol-gel syntheses in different TiO_2@ZnO composites were successfully performed. With increasing Zn doping we observed the presence of undesirable secondary phases (zinc titanate and rutile). The undesirable ATR transformation was observed even in small doping concentrations. XRD analysis and Raman spectroscopy data confirmed the partial incorporation of Zn^{2+} ions into the tetragonal structure of anatase with no distortions. SEM analysis revealed the expected spherical shape of the synthesized particles but in the form of micron-sized agglomerates. Determined band gap values of the synthesized particles confirmed that zinc presence and increasing ATR transformation lowers the band gap energy.

Acknowledgments

This paper was achieved with the financial support by the project No. CZ.02.01.01/00/22_008/0004631 (*Materials and technologies for sustainable development* within the Jan Amos Komensky Operational Program financed by the European Union) and by the project of specific research FCH-S-23-8208 (Faculty of Chemistry, Brno University of Technology).

References

[1] Sampath A H J, Wickramasinghe N D, de Silva K M N and de Silva R M. 2023 Methods of extracting TiO2 and other related compounds from ilmenite. Minerals 13 10.3390/min13050662
[2] Qiu D, Li F, Yan J, Gao W and Chong Z 2022 Machine learning for inversing FeO and TiO2 content on the Moon: Method and comparison. Icarus 373 10.1016/j.icarus.2021.114778
[3] Ikreedeegh R R, Hossen M A, Tahir M and Aziz A A 2024 A comprehensive review on anodic TiO2 nanotube arrays (TNTAs) and their composite photocatalysts for environmental and energy applications: Fundamentals, recemt advances and applications. Coordination Chemistry Reviews 499 10.1016/j.ccr.2023.215495
[4] Ratha T, Ponnanettiyappan N J and Rubensudhakar D 2021 Fabrication of visible-light assisted TiO2-WO3-PANI membrane for effective reduction of chromium (VI) in photocatalytic membrane reactor. Environmental Technology & Innovation 24 10.1016/j.eti.2021.102023
[5] Zhang Z, Sun Y, Wang Y, Yang Y, Wang P, Shi L, Feng L, Fang S, Liu Q, MA L, Peng S and Wang T 2022 Synthesis and photocatalytic activity of g-C3N4/ZnO composite microspheres under visible light exposure. Ceramics international 48 3293-3302 10.1016/j.ceramint.2021.10.104
[6] Seikh M, Pazirofteh M, Dehgani M, Asghari M, Rezakami M, Valderrama C and Cortina J L 2020 Application of ZnO nanostructures in ceramic and polymeric membranes for water and wastewater technologies: A review. Chemical Engineering Journal 391 10.1016/j.cej.2019.123475
[7] Jing Y, Yin H, Li CH, Chen J, Wu S, Liu H, Xie L, Lei Q, Sun M and Yu S 2022 Fabrication of Pt doped TiO2-ZnO@ZIF-8 core@shell photocatalyst with enhanced activity for phenol degradation. Environmental Research 203 10.1016/j.enver.2021.111819
[8] Khairy M, Kamar E M and Mousa M A 2022 Photocatalytic activity of nano-sized Ag and Au metal-doped TiO2 embedded in rGO under visible light irradiation. Materials Science and Engineering: B 286 10.1016/j.mseb.2022.116023
[9] Halin D S C, Abidin A S Z, Azani A, Salleh M A A M, Razak K A, Abdullah M M A B, Ramlu M M, Sandu A V, Vizureanu P, Kaczmarek L, Garus S and Garus J 2022 Synthesis of Zn/TiO2 Thin Films for Self-Cleaning Applications. Acta physica polonica A 142 10.12693/APhysPolA.142.164
[10] Dikici T, Yilmaz O, Akalin A, Demirci S, Gültekin S, Yildirim S and Yerddaşkal M 2022 Production of Zn-doped TiO2 film with enhanced photocatalytic aktivity. Journal of the Australian Ceramic Society 58 1415-1421 10.1007/s41779-022-00712-7
[11] Mustapha S, Tijani J O, Ndamisto M M, Abdulkareem A S, Shuaib D T, Amigun A T and Abubakar H L 2021 Fascile synthesis and characterization of TiO2 nanoparticles: X-ray peak profile analysis using Williamson-Hall and Debey-Scherrer methods. International Nano Letters 11 10.1007/s40089-021-00338-w
[12] Younis A B, Milosavljevic V, Fialova T, Smerkova K, Michalkova H, Svec P, Antal P, Kopel P, Adam V, Zurek L and Dolezelikova K 2023 Synthesis and characterization of TiO2 nanoparticles combined with geraniol and their synergistic antibacterial activity. BMC Microbiology 23 10.1186/s12866-023-02955-1
[13] Javed H M A, Adnan M, Qureshi A A, Javed S, Adeel M, Akram M A, Shahid M, Ahmad M I, Afzaal M, Abd-Rabbah H S M and Arif M 2022 Morphological, structural, thermal and optical properties of Zn/Mg-doped TiO2 nanostructures for optoelectronic applications. Optics & Laser Technology 146 10.11016/j.oplastec.2021.107566
[14] Regraguy B, Ellouzi I, Mabrouki J, Rahmani M, Drhimer F, Mahmou Ch, Dahchour A, Mrabet M E and Hajjaji S E 2022 Zinc doping of different nanoparticles of TiO2 Sachtopore for improved elimination of the methyl orange by photocatalysis. Emergent Materials 5 1945-1958 10.1007/s42247-022-00403-w
[15] Aware D V and Jadhav S S 2016 Synthesis, characterization and photocatalytic applications of Zn-doped TiO2 nanoparticles by sol-gel method. Applied Nanoscience 6 965-972 10.1007/s13204-015-0513-8
[16] Chauhan R, Kumar A and Chaudhary R P 2012 Structural and optical characterization of Zn doped TiO2 nanoparticles prepared by sol-gel method. Journal of Sol-Gel Science and Technology 61 585-591 10.1007/s10971-011-2664-8

[17] Behnajady M A, Eskandarloo H, Modirsahala N and Shorki M 2011 Investigation of the effect of sol-gel synthesis variables on structural and photocatalytic properties of TiO2 nanoparticles. Desalination 278 10-17 10.1016/j.desal.2011.04.019
[18] Bagheri S, Shameli K and Hamid S B A 2013 Synthesis and Characterization of Anatase Titanium Dioxide Nanoparticles Using Egg White Solution via Sol-Gel Method. Composite Nanoparticles 2013 10.1155/2013/848205
[19] Ke S, Cheng X, Wang Q, Wang Y and Pan Z 2014 Preparation of a photocatalytic TiO2/ZnTiO3 coating on glazed ceramic tiles. Ceramic International 40 6 8891-8895 10.1016/j.ceramint.2014.01.027
[20] Yang H, Zhang K, Shi R, Li X, Dong X and Yu Y 2006 Sol-gel synthesis of TiO2 nanoparticles and photocatalytic degradation of methyl orange in aqueous TiO2 suspensions. Journal of Alloys and Compounds 413 302-306 10.1016/j.jallcom.2005.06.061
[21] Dubey R S 2018 Temperature-dependent phase transformation of TiO2 nanoparticles synthesized by sol-gel method. Materials Letters 215 312-317 10.1016/j.matlet.2017.12.120
[22] Qian X, Gao M Y, Cao Y and Guo B L 2013 Preparation and phase structures of Zn-Ti-O ternary compounds by atomic layer deposition. Journal of Vacuum Science & Technology 31 10.1116/1.4769451
[23] Song G B, Liang J K, Liu F S, Peng T J and Rao G H 2005 Preparation and phase transformation of anatase-rutile crystals in metal doped TiO2 muscovite nanocomposites. Thin Solid Films 491 110-116 10.1016/j.tsf.2005.05.035
[24] Bartam S F and Slepetys R A 1961 Compound Formation and Crystal Structure in the System ZnO-TiO2. Journal of the American Ceramic Society 44 10 10.1111/j.1151-2916.1961.tb13712.x
[25] Monshi A, Foroughi M R and Monshi M R 2012 Modified Scherrer Equation to Estimate More Accurately Nano-Crystallite Size Using XRD. World Journal of Nano Science 2 154-160 doi:10.4236/wjnse.2012.23020
[26] Burton W, Ong K, Rea T and Chan I Y. 2009 On the estimation of average crystallite size of zeolites from the Scherrer equation: A critical evaluation of its application to zeolites with one-dimensional pore systems. Microporous and Mesoporous Materials 117 75-90 doi:10.1016/j.micromeso.2008.06.010
[27] Komaraiah D, Radha E, James J, Kalarikkal N, Sivakumar J, Reddy M V and Sayanna R 2019 Effect of particle size and dopant concentration on the Raman and the photoluminiscence spektra of TiO2: Eu3+ nanophosphor thin films. Journal of Luminescence 211 320-33 10.1016/j.lumin.2019.03.050
[28] Zhu Q, Peng Y, Lin L, Fan C, Gao G, Wang R and Xu A 2014 Stable blue TiO2-x nanoparticles for efficient visible light photocatalysts. Journal of Material Chemistry A 2 4429-4443 10.1039/c3ta14484d
[29] Arin J, Thongtem S, Phuruangrat A and Thongtem T 2016 Characterization of ZnO-TiO2 and zinc titanate nanoparticles synthesized by hydrothermal process. Research on Chemical Intermediates 43 3183-3195 10.1007/s11164-016-2818-y
[30] Sekiya T, Ohta S, Kamei S, Hanakawa M and Kurita S 2001 Raman spectroscopy and phase transition of anatase TiO2 under high pressure. Journal of Physics and Chemistry of Solids 62 717-721 10.1016/S0022-3697(00)00229-8
[31] Saravanan S and Dubey R S 2021 Optical and morphological studies of TiO2 nanoparticles prepared by sol-gel method. Materials Today: Proceedings 47 9 1811-1814 10.1016/j.matpr.2021.03.207
[32] Tamgadge Y S, Muley G G, Deshmukh K U and Pahurkar V G 2018 Synthesis and nonlinear optical properties of Zn doped TiO2 nano-colloids. Optical Materials 86 185-190 10.1016/j.optmat.2018.09.030
[33] Qiao L, Xie F, Xie M, Gong C, Wang W and Gao J 2016 Characterization and photoelectrochemical performance of Zn-doped TiO2 films by sol-gel method. Transactions of Nonferrous Metals Society of China 26 2109-2116 10.1016/S1003-6326(16)64325-X
[34] Wattanawikkam C and Percharapa W 2015 Synthesis and Characterization of Zn-Doped TiO2 Nanoparticles via Sonochemical Method. Integrated Ferroelectrics 1 167-175 10.1080/10584587.2015.1063928